AMSE JOURNALS-AMSE IIETA publication-2017-Series: Modelling B; Vol. 86; N°2; pp 471-483
Submitted Mar. 17, 2017; Revised May 11, 2017; Accepted May 25, 2017

Romax-Based Contact Analysis of Tapered Roller Bearings for Automobile Wheels

Rui Yu*, Jinshang Ni, Weiqin Shi

Changzhou Vocational Institute of Engineering, Changzhou 213164, China
(godever@gmail.com)

Abstract

Based on the simulation software of Romax and the theory of maximum orthogonal shear stress, this paper analyses the surface and subsurface contacts of double row tapered roller bearings for automobile wheels, and examines the effect of contact curvature on the maximum orthogonal shear stress of subsurface. The conclusions are as follows. The inner ring raceway has a slightly higher contact load and stress than the outer ring raceway. Under the external load, the double row tapered roller bearing exhibited a certain pitch deformation, and the second row of roller and the inner ring raceway are more prone to failure damages. With the increase of depth, the subsurface orthogonal shear stress increased first and then decreased. If the depth is kept constant, the maximum orthogonal shear stress of subsurface increased with the curvature.

Key words

Automobile wheels, Double row tapered roller bearings, Surface contact, Subsurface contact, Orthogonal shear stress.

1. Introduction

Featuring strong load bearing, sound rigidity, long service life and other advantages, the double row tapered roller bearing has infiltrated nearly every aspect of the modern life, especially in the design of automobile wheels. Due to the special working conditions and structures, strict requirements have been imposed on the bearing of automobile wheels. The bearing must be adapted to the limited height of the bearing section, and installed using the smallest possible space. With a

compact structure, light weight and large width, the double row tapered roller bearing is an ideal choice for automobile wheels. The bearing also boasts a strong load capacity. Under the same dimensions, the rated dynamic and static load of such a bearing is twice that of a double row ball bearing.

The contact properties are critical to the bearing of vehicle wheels. Any two objects in contact with each other may suffer from contact failure. Rather than limited to the contact surface, the failure is also found in the subsurface structure, as evidenced by the micro cracks at a certain depth under the surface. The cracks often expand from the surface to the subsurface, resulting in flake peeling, pitting, and ultimately the stripping failure. Such a failure is commonly referred to as subsurface origin-oriented failure [1-2]. Therefore, the contact analysis should not stop at the features of contact surface, but dig into the stress size and depth of subsurface. Nevertheless, the commonly used Hertz contact theory only applies to the surface stress resulted from the concentrated force vertically acting at the surface [3]. In order to calculate how surface stress acts on subsurface, it is necessary to introduce the calculation theory of shear stress [4-6].

Targeted at the double row tapered roller bearing for automobile wheels, this paper carries out the contact simulation and analysis of the surface and subsurface, and discusses the effect of contact curvature on the maximum orthogonal shear stress of subsurface. The research was performed based on the simulation software of Romax and the theory of maximum orthogonal shear stress.

2. Contact Theory

2.1 Surface Contact Stress

According to the Hertz contact theory, the contact area between any two contacting objects obeys the elliptical distribution (Figure 1).

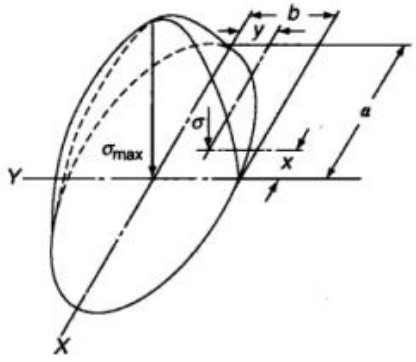

Fig.1. Hertz contact area

In Figure 1, a and b are the semi-major axis and the semi-minor axis of the elliptical contact area, respectively. If the load at the maximum stress point, i.e. the geometric enter of the ellipse, is denoted as Q, then the corresponding maximum contact stress is:

$$\sigma_{\max} = -\frac{3Q}{2\pi ab} \tag{1}$$

For a tapered roller bearing, the roller is linearly contacted with the inner and outer ring raceways, respectively. In this case, the contact area becomes a semi-elliptic cylinder, and the long axis of the ellipse approaches infinity (Figure 2). The corresponding maximum contact stress, appearing on the centreline of the cylindrical contact area, is expressed as:

$$\sigma_{\max} = \frac{2Q}{\pi lb} \tag{2}$$

where l is the length of the contact line.

The half width b of the contact area can be approximated as:

$$b = 3.35\times10^{-3}\left(\frac{Q}{l\sum\rho}\right)^{\frac{1}{2}} \tag{3}$$

where ρ is the radius of curvature.

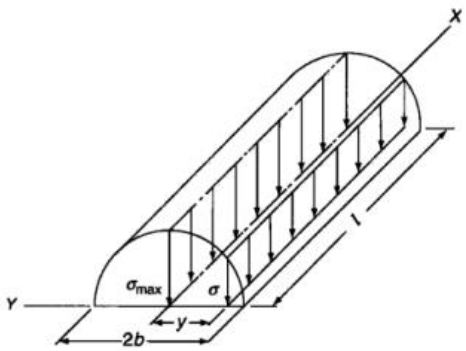

Fig.2. Linear contact area

According to formulas (2) and (3), the maximum surface contact stress of the linear contact is correlated with the length l and the radius of the semi-minor axis b of the linear contact area; the radius of the semi-minor axis b is dependent on the radius of curvature corresponding to the contact area. Whereas the roller length l is limited to a small range by the weight, cost and width of the bearing, the curvature is the most important influencing factor of the contact stress of bearing during the design process.

2.2 Subsurface Contact Stress

As mentioned before, the Hertz contact theory is only suitable for the surface stress caused by the concentrated force vertically acting on the contact surface. In actual practice, however, contact failure often originates from some points beneath the surface. Such a failure is called subsurface failure. Therefore, it is very meaningful to determine the stress size and depth of subsurface. The results can reflect if the hardness and depth are as required. The existing theories on the stress in subsurface failure mainly include the maximum shear stress theory, the maximum orthogonal shear stress theory, and the synthetic shear stress theory. Among them, the maximum orthogonal shear stress theory is the most popular and recognized strategy in the calculation of subsurface contact stress and measurement of subsurface failure [7]. It should be noted that researchers have not reached a consensus on which of the stresses is the main reason of subsurface failure.

Proposed by Palmgren and Lundberg, the maximum orthogonal shear stress theory goes as:

$$\frac{2\tau_y}{\sigma_{\max}} = \frac{(2\,\mathrm{t}-1)^{1/2}}{t(\mathrm{t}+1)} \tag{4}$$

Hence, the maximum orthogonal shear stress at the depth of z can be expressed as:

$$z = \frac{b}{(\mathrm{t}+1)(2\,\mathrm{t}-1)^{1/2}} \tag{5}$$

where t is an auxiliary parameter satisfying the following relationship:

$$\frac{b}{a} = [(\mathrm{t}^2-1)(2\,\mathrm{t}-1)]^{1/2} \tag{6}$$

To sum up, the subsurface contact stress and depth should be calculated based on the radius of semi-minor axis b of the maximum surface contact stress and surface contact area.

2.3 Curvature and Calculation Theory

As shown in Figure 3, the various contact points between the raceways and the roller share similar curvature radiuses, making it possible to use the approximate curvature and calculation formula. The curvatures and formulas of the contact area with the inner and outer ring raceways are respectively:

$$\begin{cases} \sum \rho_i = \dfrac{1}{D_m}\left(\dfrac{2}{1-r_i}\right) \\ \sum \rho_o = \dfrac{1}{D_m}\left(\dfrac{2}{1+r_o}\right) \end{cases} \tag{7}$$

where

$$\begin{cases} D_m = \dfrac{1}{2}(\mathrm{D_{max}} + \mathrm{D_{min}}) \\ \mathrm{r_i} = \dfrac{D_m \cos\alpha_i}{d_m} \\ \mathrm{r_o} = \dfrac{D_m \cos\alpha_o}{d_m} \end{cases} \tag{8}$$

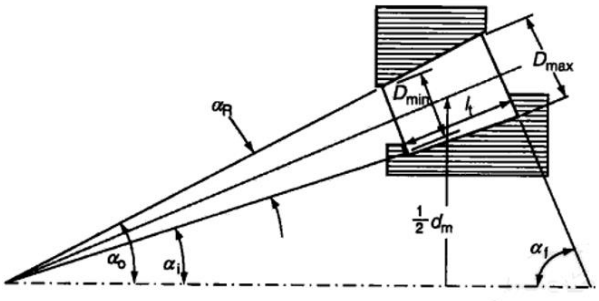

Fig.3. Curvature and geometric relationship of tapered roller bearing

3. Model Building

Capable of withstanding the axial force and radial force at the same time, the double row tapered roller bearing has been widely used in auto-making, heavy machinery, shipbuilding, military and other fields. In this research, the author attempts to model a double row tapered roller bearing for the wheels of a vehicle (Figure 4). The basic parameters and properties of the bearing are presented in Table 1. The bearing consists of a fixed outer ring and a rotating inner ring. To simulate the accurate bearing load, a hollow shaft was designed in the inner ring. The load applied on the bearing is shown in Table 2.

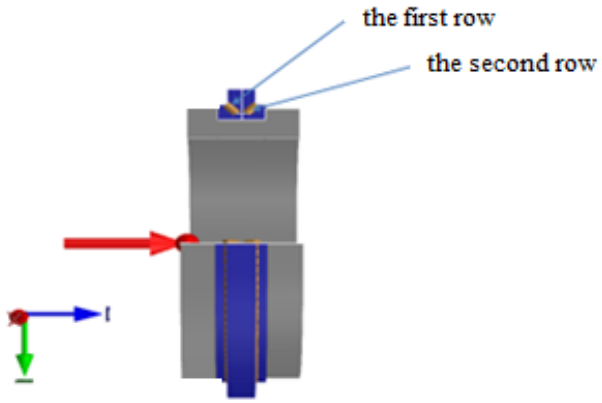

Fig.4. The analysis model

Tab.1. Basic Parameters of the bearing

Parameters	Value
Outer diameter of bearing	2800 mm
Inner diameter of bearing	2300 mm
Width of bearing	300 mm
Number of rollers in a single row	101
Contact angle	45°
Yield strength	4000MPa
Elastic modulus	2.10E5MPa
Poisson's ratio	0.3

Tab.2. Load conditions

MY	-7000KN·m
MZ	1500KN·m
FX	400KN
FY	100KN
FZ	-1500KN

4. Analysis of Contact Features

4.1 Surface Contact

To obtain the stress distribution between rollers and ring raceways, the circumferential loads on the contacts between the two rows of rollers and the inner and outer ring raceways were extracted respectively with Romax.

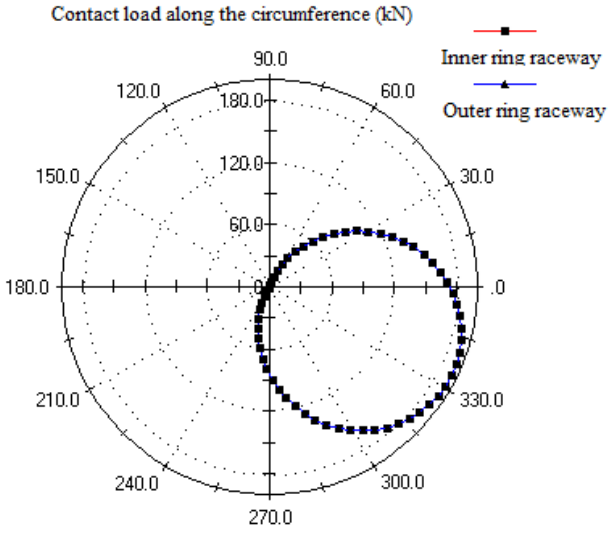

5(a). Contact loads between the first row of rollers and the inner and outer ring raceways

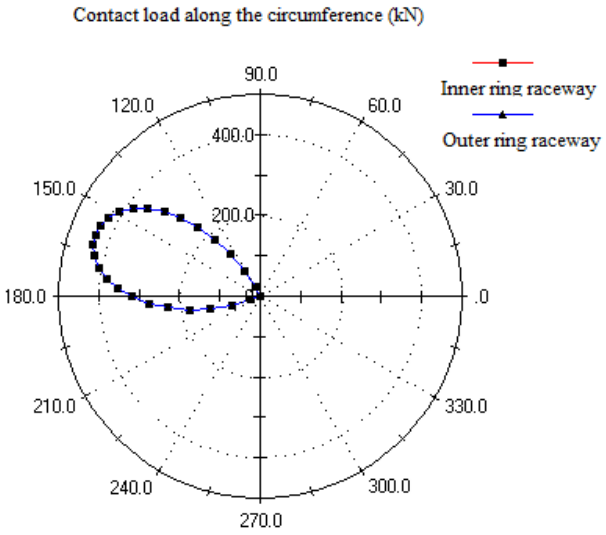

5(b). Contact loads between the second row of rollers and the inner and outer ring raceways

Fig.5. Contact loads between rollers and the inner and outer ring raceways

According to Figure 5, the distribution form and area of contact stress are basically the same with load distribution. In Figure 5(a), the contact load between the first row of rollers and the inner ring raceway occurred in [0°, 60°] and that between the first row of rollers and the outer ring raceway appeared in [240°, 360°]. The load mainly concentrated in [300°, 360°], and peaked at

192kN at the angular position of 331°. In Figure 5(b), the contact loads between the second row of rollers and the inner ring raceway both occurred in [120°, 210°]. The load mainly concentrated in [150°, 180°], and peaked at 431kN at the angular position of 158°.

Therefore, the double row tapered roller bearing exhibited a certain pitch deformation under the action of the external load. In addition, the second row of rollers and raceways are the main bearing parts of the bearing structure, with a maximum load 2~3 times of that of the first row of rollers and a relatively narrow scope of action.

The circumferential contact loads between the two rows of rollers and the inner and outer ring raceways were extracted respectively with Romax. Then, the distribution diagram of the contact stress between rollers and raceways was established with the angular position as the horizontal coordinate and the roller length as the vertical coordinate (Figure 6).

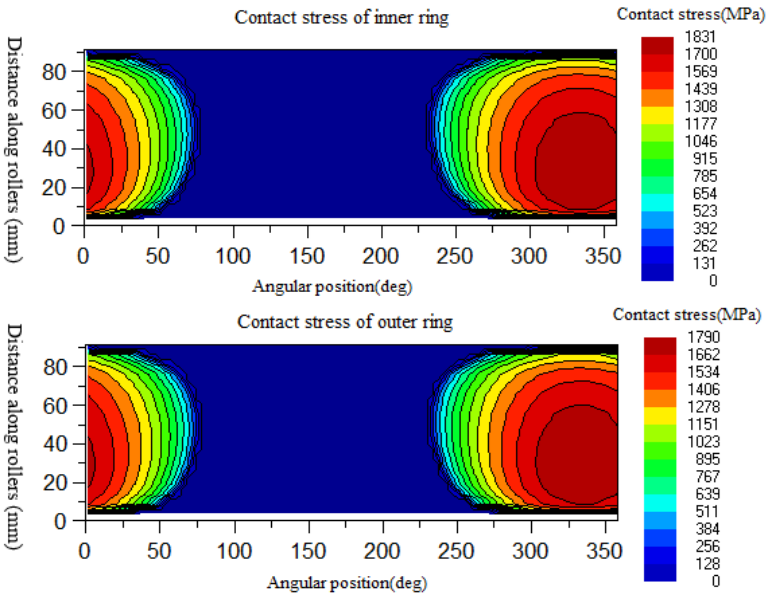

6(a). Contact stress between the first row of rollers and the inner and outer ring raceways

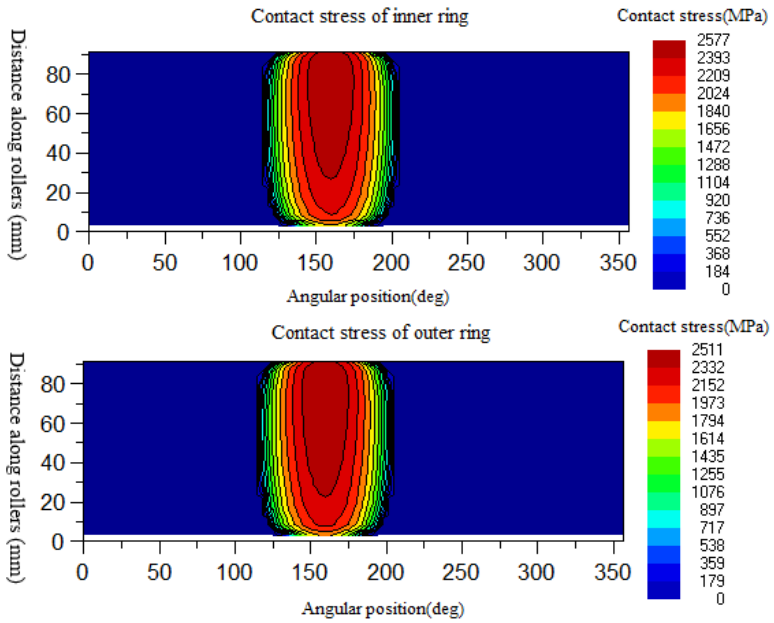

6(b). Contact stress between the second row of rollers and the inner and outer ring raceways

Fig.6. Surface contact stress

As can be seen from Figure 6, the contact stress was generated between the rollers and inner/outer ring raceway under the action of roller and the load of raceway, the contact stress was distributed in a similar form and area with the contact load, and the inner ring raceway has a slightly higher contact stress than the outer ring raceway. Through comparison, it is clear that the second row of roller, with a narrower contact area, was under a far greater contact stress than the first row of rollers, and was more likely to suffer from failure damage. Table 3 shows the maximum contact load, the maximum contact stress, semi-minor axis of the elliptical contact, position and other information of the first and second row of rollers and inner/outer raceways. To analyse the subsurface contact, the author probed into the contact between the more failure-prone second row of rollers and the inner ring raceway.

Tab.3. Maximum contact results

	The first row	The second row
Maximum contact load of roller	192KN	431KN
Position of maximum contact load of roller	Counter-clockwise 331°	Counter-clockwise 158°
Maximum surface contact stress	1831MPa	2577MPa
Maximum elliptical minor semi-axis of surface contact	970um	1301um
Position of maximum surface contact stress	Counter-clockwise 331°	Counter-clockwise 158°

4.2 Subsurface Contact

According to the maximum orthogonal shear stress theory provided by Palmgren and Lundberg, the computed result of the surface contact between the second row of rollers and inner ring raceway is substituted to obtain the change of subsurface stress of contact between the second row of rollers and inner ring raceway along with the change in depth, as shown in Table 4. The changing curve of maximum orthogonal shear stress of the corresponding subsurface is shown in Figure 7.

It can be seen from Table 4 and Figure 7 that: with the increase of depth, the subsurface orthogonal shear stress increased first and then decreased; the maximum orthogonal shear stress reached 723MPa at the depth of 1.04mm. In actual design, if the depth is kept at 1.04mm, the shear stress permitted by the bearing hardness is greater than 723MPa. Hence, a safety coefficient should be introduced according to the actual situation.

Tab.4. Subsurface stress variation with depth

Curvature	0.034	
Z/b	Depth z (mm)	τ
0	0	0
0.2	0.2602	388.068
0.4	0.5204	605.004
0.6	0.7806	701.412
0.8	1.0408	723.108
1	1.301	706.236
1.5	1.9515	607.416
2	2.602	508.584
2.5	3.2525	431.46
3	3.903	371.196
4	5.204	286.836
5	6.505	233.808
6	7.806	197.652
8	10.408	149.436
10	13.01	120.516
15	19.515	79.548
20	26.02	60.264
Max	1.0408	723.108

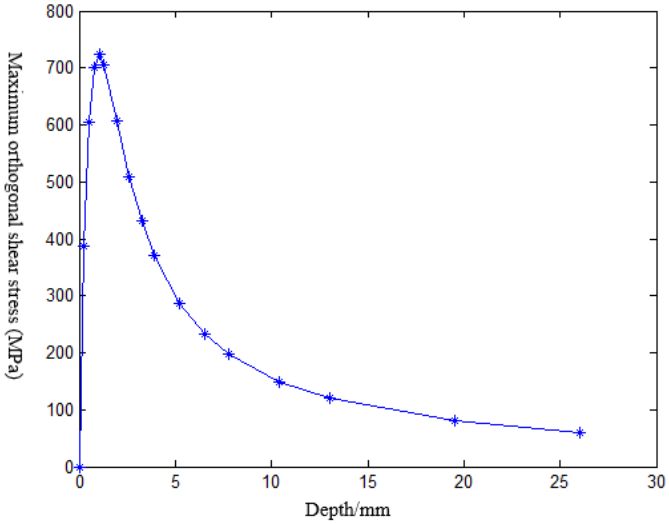

Fig.7. Surface stress variation curve

Next, the author explored the effect of bearing curvature on the orthogonal shear stress of subsurface contact. The contact curvature of bearing was changed to 0.035, 0.036 and 0.037, respectively, to extract the corresponding maximum orthogonal shear stresses (Figure 8). As shown in Figure 8, if the depth is kept constant, the maximum orthogonal shear stress of subsurface increased with the curvature.

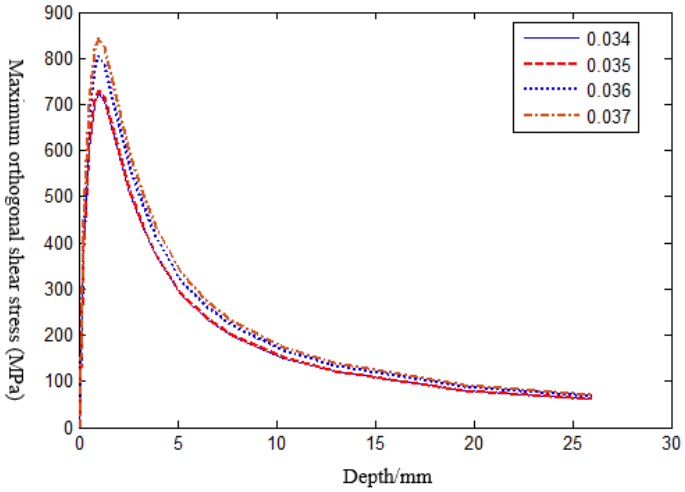

Fig.8. Maximum orthogonal subsurface shear stress at different curvatures

Conclusion

Through the analysis on the surface and subsurface contacts of double row tapered roller bearings for automobile wheels, the author drawn the following conclusions:

(1) The double row tapered roller bearing exhibited a certain pitch deformation under the action of the external load. In addition, the second row of rollers and raceways are the main bearing parts of the bearing structure, with a relatively narrow scope of action.

(2) The distribution form and area of contact stress are basically the same with load distribution, the inner ring raceway has a slightly higher contact load and stress than the outer ring raceway, and the second row of roller and the inner ring raceway are more prone to failure damages.

(3) With the increase of depth, the subsurface orthogonal shear stress increased first and then decreased; In actual design, the shear stress permitted by the bearing hardness is greater than the maximum orthogonal shear stress.

(4) If the depth is kept constant, the maximum orthogonal shear stress of subsurface increased with the curvature.

All in all, this paper digs deep into the theory and contact of double row tapered roller bearing for automobile wheels, providing an important reference to the optimization of the design, the improvement of the bearing capacity and the reduction of the vibration noise.

Acknowledgement

This work is supported by Top-notch Academic Programs Project of Jiangsu Higher Education Institutions (PPZY2015C235).

References

1. J. Lai, K. Stadler, Investigation on the mechanisms of white etching crack (WEC) formation in rolling contact fatigue and identification of a root cause for bearing premature failure, 2016, Wear, no. s364–365, pp. 244-256.
2. J. Gegner, W. Nierlich, Comparison of the Microstructural Changes and X-ray Diffraction Peak Width Decrease during Rolling Contact Fatigue in Martensitic Microstructures, 2012, Symposia Papers & STPs.
3. X.Y. Meng, Mechanical analysis on subsurface peeling of rollers of Baosteel' s four-roll cold-rolling mill and reasonable determination of surface hardening depth of working rollers and regrinding amount of support roller, 1995, Metallurgical Equipment, no. 5, pp. 6-12.
4. M.H. Evans, A.D. Richardson, L. Wang, R.J.K. Wood, Serial sectioning investigation of butterfly and white etching crack (WEC) formation in wind turbine gearbox bearings, 2013, Wear, vol. 302, no. 1–2, pp. 1573-1582.

5. L. Shi, Cause analysis of low subsurface hardness of carburized gear, 1998, Metal Heat Treatment, no. 8, pp. 28-29.
6. D.L. Sun, X.F. Qin, L.Y. Xie, W.U. Qiong, Impact of friction coefficient on subsurface contact fatigue damage of supporting rollers, 2014, Journal of Northeastern University (Natural Science Edition), vol. 35, no. 5, pp. 731-734.
7. T.A. Harris, M.N. Korzalas, Analysis of rolling bearing, volume 1, basic concept of bearing technology, 2010, Machinery Industry Press.
8. N. Boubaya, B. Saad, M. Maazouz, Radial active magnetic bearing control using fuzzy logic, 2016, Modelling, Measurement and Control A, vol. 89, no. 1, pp. 92-100.
9. N. Liu, Z.C. Zheng, G.X. Li, Analysis of diesel engine main bearing lubrication under single-cylinder misfiring situation, 2015, International Journal of Heat and Technology, vol. 33, no. 4, pp. 85-90.
10. W.Q. Sun, J. Shao, A.R. He, H.S. Zhao, J Zhou, Research on residual stress quantitative reduction in laminar cooling on hot strip mill, 2015, International Journal of Heat and Technology, vol. 33, no. 4, pp. 19-24.
11. H.C. Jing, Coverage holes recovery algorithm based on nodes balance distance of underwater wireless sensor network, 2014, International Journal on Smart Sensing and Intelligent Systems, vol. 7, no. 4, pp. 1890-1907.